Check for updates

Geometries and stabilities of chromium doped nitrogen clusters: mass spectrometry and density functional theory studies†

Zaifu Jiang,‡[a] Peixin Fu,‡[ab] Meicheng Chen,[c] Chen Chen,[c] Bole Chen,[d] Wei Dai,[a] Kewei Ding [ID] *[ef] and Cheng Lu [ID] *[c]

Metal-doped nitrogen clusters serve as effective models for elucidating the geometries and electronic properties of nitrogen-rich compounds at the molecular scale. Herein, we have conducted a systematic study of VIB-group metal chromium (Cr) doped nitrogen clusters through a combination of mass spectrometry techniques and density functional theory (DFT) calculations. The laser ablation is employed to generate CrN_n^+ clusters. The results reveal that CrN_8^+ cluster exhibits the highest signal intensity in mass spectrometry. The photodissociation experiments with 266 nm photons confirm that the chromium heteroazide clusters are composed of chromium ions and N_2 molecules. Further structural searches and electronic structure calculations indicate that the cationic CrN_8^+ cluster possesses an X shaped geometry with D_2 symmetry and exhibits robust stability. Molecular orbital and chemical bonding analyses demonstrate the existence of strong interactions between Cr^+ cation and N_2 ligands. The present findings enrich the geometries of metal doped nitrogen clusters and provide valuable guidance for the rational design and synthesis of novel transition metal nitrides.

1 Introduction

Metal atoms, including transition metals (TMs), incorporated into nitrogen cluster nanoparticles are recognized as potential high-energy-density materials due to substantial energies released during the fragmentation reactions.[1–6] Compared to pure nitrogen clusters, which suffer from poor stabilization and challenging preparation processes, metal-doped nitrogen clusters exhibit distinctive properties. Normally, the nitrogen skeletons are prone to enhance their stabilities through bonding with the metal atoms and their structures show diversity, making them environmentally friendly high-energy-density

material candidates.[7–10] Thus, the investigations on the varied geometries and structural stabilities of metal-doped nitrogen clusters have attracted much attention. Ongoing efforts focus on understanding the distinct structural patterns and evolutions guided by different metal-doped nitrogen clusters, with the goal of elucidating the interactions and bonding mechanisms between the metal atoms and the main nitrogen ligands.

So far, researchers have conducted extensive studies on metal-doped nitrogen clusters through diverse experimental and theoretical methods. For example, N_4 rings doped with alkaline earth metals (M = Ca^{2+}, Sr^{2+}, Ba^{2+}) exhibit pyramidal structures.[11] The syntheses of numerous binary azides, including group 4 elements (like Ti), group 5 elements (such as V, Nb and Ta),[12–14] group 6 elements (Mo and W),[15] group 15 element (Bi)[16] and so on, were systematically explored through experimental methods. Gagliardi *et al.*[17] identified a local minimum isomer with C_{7v} symmetry for ScN_7 in Sc-doped N clusters and demonstrated the local stability of sandwich geometric structures in TM-doped N_5MN_7 (M = Ti, Zr, Hf, Th) clusters. In addition, the geometries and stabilities of numerous metal-doped polyazides (*e.g.*, tri-azides $M(N_3)_3$ (M = Sc, Y, La, Al, Ga, In, Tl)[18–20] of group 3 and 13, tetra-azides $M(N_4)_3$ (M = Ti, Zr, Hf, Th, Ge, Sn, Pb)[18,21] of group 4 and 14, as well as novel aromatic compounds with planar N_6 rings of ScN_6^-, VN_6^+, Ca_2N_6, ScN_6 Cu and $M(\eta^6-N_6)$ (M = Ti, Zr, Hf, Th)[22,23] and so on), have been extensively studied both experimentally and theoretically.

[a] *School of Mathematics and Physics, Jingchu University of Technology, Hubei 448000, China*

[b] *Department of Physics and Optoelectronic Engineering, Yangtze University, Jingzhou 434023, China*

[c] *School of Mathematics and Physics, China University of Geosciences (Wuhan), Wuhan 430074, China. E-mail: lucheng@calypso.cn*

[d] *School of Science, Chongqing University of Posts and Telecommunications, Chongqing 400065, China*

[e] *Xi'an Modern Chemistry Research Institute, Xi'an 710065, China. E-mail: dkw204@163.com*

[f] *State Key Laboratory of Fluorine & Nitrogen Chemicals, Xi'an 710065, China*

† Electronic supplementary information (ESI) available. See DOI: https://doi.org/10.1039/d4cp01203h

‡ These authors contributed equally to this work and should be considered as co-first authors.

In particular, in 2017, Zhang *et al.*[2] successfully synthesized the pentazolate anion cyclo-N_5^-, revealing its unexpected stability and potential application in energetic polynitrogen compounds. Subsequently, Sun *et al.*[24] achieved a significant breakthrough in cyclo-pentazole chemistry by experimentally isolating the AgN_5 of the cyclo-N_5^- metal complex. Wang *et al.*[25] reported the synthesis of planar N_6^{2-} hexazine dianions through potassium azide (KN_3) under high pressure. Laniel *et al.*[26] conducted a study on the synthesis of the K_9N_{56} compound by laser heating under high pressure and a first principles calculations. The results revealed that the K_9N_{56} compound comprises a complex arrangement of planar aromatic hexazine $[N_6]^{4-}$ and $[N_5]^-$ rings, along with neutral nitrogen dimers. Moreover, the diverse properties exhibited by metal-doped nitrogen clusters of varying sizes have stimulated scientists to systematically explore the size-dependent properties of these clusters. In recent years, there has been a surge of in-depth studies focusing on the alkali metal hetero-azide clusters, specifically LiN_n^+ and $Li_2N_n^+$,[27–29] as well as potassium heteroazide clusters (KN_n^+),[30] and sodium heteroazide clusters (NaN_n^+).[29] Substantial advancements and notable progress have been achieved.

Except for the main group elements, other attentions were directed towards the TM-doped nitrogen clusters, *i.e.* MN_n^+ (M = Sc, Zr, V, Cu, Fe, Co, Ni, Ti, Zn),[31–35] which focus on the generations and geometries of these clusters, shedding light on their structure and electronic properties. These findings verify the imperative for further exploration of the structures and characteristics of metal-doped nitrogen clusters. A deeper comprehension of the bonding modes between metal and nitrogen atoms holds promise for the rational design of stabilizers and catalysts tailored for all-nitrogen materials. Overall, these studies reveal the profound impact of metal doping, including transition metals, in modulating the geometric and electronic properties of nitrogen clusters, unveiling unique properties distinct from their bulk materials.

Cr is the inaugural element in group 6 of the periodic table, which exhibits distinctive physical properties, presenting as a steely-grey, lustrous, hard, and brittle transition metal. The $[Ar]3d^5 4s^1$ electronic configuration of Cr fosters the formation of robust d–d bonds and notably short bond lengths (1.68 Å) in its dimers.[36,37] Beyond its inherent electronic properties, Cr holds significance in industrial applications, engaging in interactions with non-metallic elements such as oxygen,[38] carbon,[39] and nitrogen.[39–41] The versatility of Cr enhances its value, making it advantageous for applications as the catalyst or the coating for hard materials. Wang *et al.*[42] uncovered the nitrogen-induced magnetic transition of Cr atom in their exploration of Cr_mN (m = 2–5) and Cr_2N_2. Specifically, the neighboring Cr atom exhibited antiferromagnetic coupling to nitrogen, causing the robust Cr–N bonds. The study of Cr doped nitrogen clusters also contributes to the understanding of the structural evolution and formation mechanisms of nitrogen rich compounds at the atomic and molecular levels. Some of them are expected to serve as precursors for energy-containing materials or the synthesis of nitrogen-riched

materials. Consequently, there is an intriguing impetus to study Cr doped nitrogen clusters and explore their unconventional chemical bonding patterns. This work involves a systematic study of Cr doped nitrogen clusters using laser sputtering and photolysis techniques in combination with DFT calculations. The objective is to achieve a comprehensive understanding of the structural evolutions and stabilities of Cr doped nitrogen clusters.

2 Methods

The experiments were conducted employing a custom-designed laser sputtering-time-of-flight (TOF) mass spectrometer.[43] The apparatus comprises a Nd:YAG laser, a laser sputtering ion source, a reflectance TOF mass spectrometer, a vacuum system, a carrier gas system, and a timing system, *etc.* It was successfully applied to prepare various metal doped nitrogen clusters.[28,32–34] Firstly, solid samples with a diameter of 13 mm and a thickness of 2–5 mm were fabricated using a tablet press, employing a Cr/AlN mole ratio of 2 : 1. Subsequently, the surface of the samples underwent pulsed laser sputtering on a laser sputtering-TOF mass spectrometer to generate chromium hetero nitrogen clusters. High-purity nitrogen served as the carrier gas during this process to facilitate the formation of chromium-hybrid nitrogen clusters, while liquid nitrogen was employed to cool the clusters generated by laser bombardment. The laser system was characterized by specific operational parameters, namely a wavelength of 532 nm, a pulse energy of approximately 10 mJ, and a repetition frequency of 10 Hz. At a pressure of approximately 4 atmospheres, nitrogen was introduced into the source region through a pulse valve (General Valve Series 9) to cool the clusters formed. The synthesized Cr doped nitrogen clusters were acceleration, deflection, and focusing with the carrier gas in the high-voltage electric field acceleration region, reaching the reflection region, and finally arriving at the microchannel plate (MCP) detector of the TOF mass spectrometer after reflection. Signals from the detectors were passed through a preamplifier and recorded by a 200 MHz digital acquisition card. The acquired digital data were subsequently organized and analyzed using self-programmed software. In addition, CrN_8^+ cluster, which exhibits the stronger peak in mass spectra of the generated chromium heteroazide clusters, was photolysed with a laser at a wavelength of 266 nm using a mass gate in a time-of-flight mass spectrometer, and mass spectra of the photolysed products were obtained.

The systematic search of the potential energy surfaces (PESs) of neutral and cationic $CrN_n^{0/+}$ (n = 2–11) were performed using the CALYPSO package.[44–46] The CALYPSO package is based on the particle swarm optimization (PSO) method, which is very efficient in prediction structure of various cluster systems,[47–52] including boron clusters[48] and nitrogen clusters.[34,47] After cluster structural searches, numerous of neutral and cationic $CrN_n^{0/+}$ with were obtained. We then selected candidate isomers for re-optimization based on the following criteria: (a) the isomer with relative lower energy less than 3 eV compared to

This journal is © the Owner Societies 2024

Phys. Chem. Chem. Phys., 2024, **26**, 14538–14546 | **14539**

the lowest-energy structure. (b) The isomer with high symmetry. (c) The isomers with variegated geometries. Subsequently, the selected structures were re-optimized at the high-accuracy level of M06-2X/6-311+G(d,p), which was verified to be reliable in various DFT calculations of metal doped nitrogen clusters. The calculated bond length of N_2 molecular is 1.090 Å which is in agreement with the experimental value of 1.097 Å.[53] For each isomer, various spin multiplicities (doublet, quartet, sextet for neutrals and singlet, triplet, quintet for cations) were considered. During the geometric optimizations, the vibration frequencies were considered for all low-lying isomers to ensure that the structures are stable and without imaginary frequencies. Chemical bonding analyses were performed using the natural bond orbital (NBO) and adaptive natural density partitioning (AdNDP) methods[54] to gain deeper insights into bonding characteristics. All computations were carried out using the Gaussian 09 package.[55]

3 Results and discussions

As depicted in Fig. 1(a), the chromium–nitrogen clusters produced by laser bombardment of Cr/AlN samples are mainly CrN_6^+, CrN_8^+, CrN_9^+, and CrN_{11}^+ clusters. Notably, the signal intensity of CrN_8^+ cluster is significantly higher than that of other chromium–nitrogen clusters. This observation suggests that CrN_8^+ cluster represents the most stable isomer among the synthesized chromium–nitrogen clusters. In addition, mass spectral peaks of a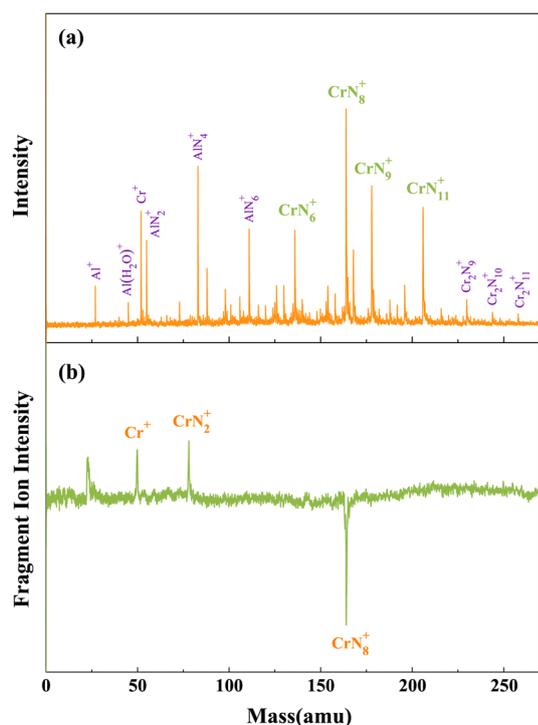luminum–nitrogen clusters, specifically AlN_2^+, AlN_4^+ and AlN_6^+ are observed due to the presence of aluminum impurities. Then, laser photolysis of CrN_8^+ cluster is performed at 266 nm, as shown in Fig. 1(b). The cationic CrN_8^+ cluster exhibits two dissociation channels: one involving the loss of six N atoms, resulting in the production of CrN_2^+ fragment ions, and the other involving the loss of eight N atoms, leading to the generation of Cr^+ fragment ions.

The geometries, symmetries, spin multiplicities and relative energy differences of neutral and cationic chromium–nitrogen clusters are presented in Fig. 2 and 3, respectively. Each isomers of the neutral chromium–nitrogen cluster are labeled as na, nb, and nc (na$^+$, nb$^+$, and nc$^+$ for cations), where n represents the number of N atoms in isomers. The letters a, b, and c (a$^+$, b$^+$, and c$^+$) denote the energy order of the isomers, respectively. By considering vibration frequencies, all the shown structures are identified to be stable. The calculated total energies and minimum frequencies of ground state and metastable isomers of chromium–nitrogen clusters are listed in Tables S1 and S2 of the ESI.† In addition, the electronic states of the ground state isomers are listed in Table 1.

The geometries of neutral CrN_n (n = 2–11) clusters are illustrated in Fig. 2. As for CrN_2 cluster, the 2a ground state is a stable linear Cr–N–N configuration with electronic state of $^5\Sigma$ and $C_{\infty v}$ symmetry. Two metastable 2b and 2c isomers with C_{2v} symmetry are identified, representing a planar triangular geometry and an N–Cr–N nonlinear structure, respectively. The most stable structure of CrN_3 cluster is 3a, wherein the Cr atom is nonlinearly attached to the N_3 chain, exhibiting C_S symmetry.

Fig. 1 (a) Mass spectra of $CrN_n^{0/+}$ clusters produced by laser bombardment of Cr/AlN samples. (b) Photolysis mass spectra of CrN_8^+ cluster at 266 nm.
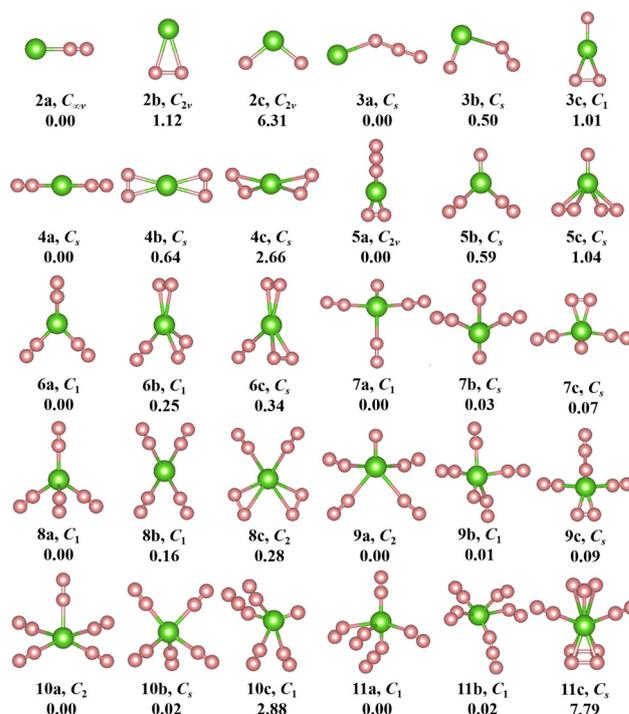

Fig. 2 The geometries, symmetries and relative energies (in eV) of optimized neutral CrN_n clusters (n = 2–11) at the M06-2X/6-311+G(d,p) level. The green and pink spheres represent Cr and N atoms, respectively.
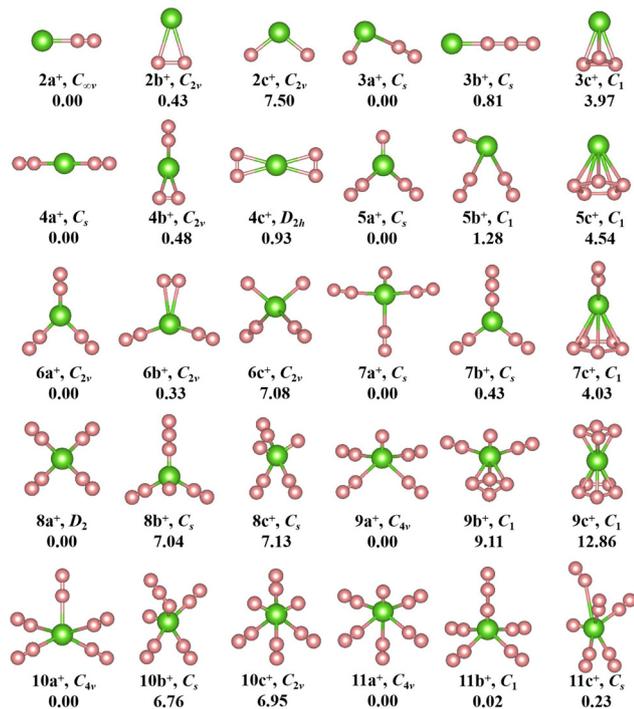
14540 | *Phys. Chem. Chem. Phys.*, 2024, **26**, 14538–14546

This journal is © the Owner Societies 2024

Fig. 3 The geometries, symmetries and relative energies (in eV) of optimized cationic CrN_n^+ clusters (n = 2–11) at the M06-2X/6-311+G(d,p) level. The green and pink spheres represent Cr cation and N atoms, respectively.

Table 1 Electronic state, E_b (eV), Δ^2E (eV) and charges Q(Cr) (e) distributed on Cr atom for the low-lying $CrN_n^{0/+}$ clusters

	CrN_n				CrN_n^+			
n	State	E_b	Δ^2E	Q(Cr)	State	E_b	Δ^2E	Q(Cr$^+$)
2	$^5\Sigma$	0.32		0.01	$^6\Sigma$	0.78		0.99
3	$^6A'$	−1.00	−3.57	0.75	$^3A''$	−1.37	−6.57	1.06
4	$^5A'$	0.13	3.01	−0.08	$^6A'$	0.84	6.55	0.89
5	$^6A_1$	−0.40	−2.65	0.80	$^3A''$	−0.46	−6.19	0.85
6	^5A	0.14	3.13	0.38	$^6A_1$	0.75	6.00	0.81
7	^4A	−0.38	−3.72	0.28	$^3A''$	−0.11	−5.80	0.61
8	$^5A'$	0.17	3.86	0.35	^6A	0.70	6.00	0.67
9	^4A	−0.27	−3.74	0.26	$^3A_2$	−0.01	−5.91	0.52
10	^5B	0.14	2.59	0.27	$^6A_2$	0.61	5.82	0.57
11	^6A	−0.01		0.58	$^3A_2$	0.06		0.41

The corresponding electronic state is $^6A'$. For n = 4, the ground state 4a ($^5A'$ electronic state) also possesses C_S symmetry and constitutes a linear N_2–Cr–N_2 geometry derived by adding the N_2 unit to 2a. The replacement of the single N atom at the topmost part of 3c by the N_3 chain leads to the formation of 5a. It is C_{2v} symmetry with $^6A_1$ electronic state. In the CrN_6 cluster, the ^5A-6a ground state exhibits low symmetry of C_1, resembling a herringbone geometry similar to 5b, with the central Cr atom attached to three N_2 units. The geometry of 7a (electronic state ^3A) in the CrN_7 cluster is characterized by C_1 symmetry, where the central Cr atom is linked by three N_2 units and an isolated N atom. For CrN_8 cluster, the $^5A'$-8a ground state is C_S symmetry and adopts an orthotetrahedral geometry containing

four N_2 ligands. In the case of n = 9, the lowest energy isomer 9a assumes the configuration of $CrN(N_2)_4$ with ^4A electronic state and C_1 symmetry. The ground state isomer of CrN_{10} cluster is 10a. It is C_2 symmetry formed by the addition of the N_2 unit to the 8b isomer, which exhibits a spread-eagled shape, representing the configuration of $Cr(N_2)_5$. As for CrN_{11} cluster, the most stable isomer is 11a (^6A, C_1) with the configuration of $CrN_3(N_2)_4$, which contains a N_3 chain similar to 3a and 5a.

The geometries of cationic CrN_n^+ (n = 2–11) clusters are depicted in Fig. 3. The ground state structure of cationic CrN_2^+ clusters, like neutral CrN_2 cluster, is 2a$^+$ isomer. It is stable linear Cr–N–N geometry with $C_{\infty v}$ symmetry. Two additional low-lying isomers are also observed: the planar triangular structure 2b$^+$ and the nonlinear N–Cr–N structure 2c$^+$. Both exhibit C_{2v} symmetry. In CrN_3^+ cluster, the ground-state 3a$^+$ is similar to neutral 3b isomer, containing an isolated N atom and an N_2 unit. It is C_S symmetry and the corresponding electronic state is $^3A''$. The 3a ground state of neutral CrN_3 undergoes a structural transition from a nonlinear geometry to a linear structure 3b$^+$ (Cr$^+$–N_3) after the loss of one electron. For CrN_4^+ clusters, like neutral isomer 4a, the ground state is 4a$^+$ ($^6A'$) with C_S symmetry, which is also a linear N_2–Cr–N_2 structure. Similar to the neutral 5b isomer, the most stable structure of the CrN_5^+ cluster is 5a$^+$. Its electronic state is $^3A''$. It is characterized by a herringbone shape with C_S symmetry. In the case of n = 6, the $^6A_1$-6a$^+$ ground state contains three N_2 units, similar to the neutral 6a, but exhibits a herringbone geometry with C_{2v} symmetry. For CrN_7^+ cluster, the geometry of the $^3A''$-7a$^+$ ground state assumes an X-like shape of Cr$^+$ N(N_2)$_3$, characterized by higher C_S symmetry compared to the neutral 7a. Similar to 7a, 8b, and 7a$^+$, the ground state isomer 8a$^+$ (electronic state ^6A) with D_2 high symmetry features the standard X-shape, where four N_2 molecules interact equitably with the central Cr atom through their terminal nitrogen atoms. The ground state of CrN_n^+ (n = 9–11) clusters, $^3A_2$-9a$^+$, $^6A_2$-10a$^+$ and $^3A_2$-11a$^+$, exhibit a similar spread-eagled shape with the same C_{4v} symmetry, which are characterized by Cr$^+$ N(N_2)$_4$, Cr$^+$ (N_2)$_5$, and Cr$^+$ N(N_2)$_5$, respectively.

Interestingly, the most stable structures of $CrN_n^{0/+}$ (n = 2–11) clusters, where n is even, the distinctive conformations, $Cr(N_2)_{n/2}$ (or $Cr^+(N_2)_{n/2}$), are observed, which are characterized by N atoms interacting with the central Cr ion through the N_2 ligands. Meanwhile, it is noted that the most stable isomers of neutral CrN_n (n = 2–11) clusters transition from one-dimensional linear ($C_{\infty v}$-2a, C_S-4a) to two-dimensional branching (C_1-6a) and further to three-dimensional tetrahedral (C_S-8a) and square pyramid (C_2-10a) configurations with the increase of number of N_2 units, whereas the most stable isomers of cationic CrN_n^+ (n = 2–11) clusters transform from one-dimensional linear ($C_{\infty v}$-2a$^+$, C_S-4a$^+$) to two-dimensional branching (C_{2v}-6a$^+$, D_2-8a$^+$) and finally to three-dimensional square pyramid (C_{4v}-10a$^+$) configurations. When the number of N atoms is odd (except for CrN_3, CrN_5 and CrN_{11}), the N atoms are connected to the Cr atom to form the configurations of $CrN(N_2)_{(n-1)/2}$ (or $Cr^+N(N_2)_{(n-1)/2}$). These findings indicate that the chromium–nitrogen clusters are composed of Cr atom

This journal is © the Owner Societies 2024

Phys. Chem. Chem. Phys., 2024, **26**, 14538–14546 | **14541**

(or Cr^+ ion) and N_2 molecules. The isomer with more number of N_2 units usually exhibit relatively lower energies than the isomer with all-nitrogen units, such as the cationic CrN_9^+ cluster. Similar results were reported by Ding *et al.*[28,33,34] for other metal doped nitrogen clusters. Notably, on the one hand, although the loss of an electron changes the spin multiplicity of chromium–nitrogen cluster, the geometrical symmetries and electronic states of $2a^+$ and $4a^+$ cations remain unchanged compared to their corresponding neutral ground states. On the other hand, in 3a, 5a and 11a, nitrogen units interact with Cr atoms in forms of N_3 chains and N_2 ligands. In addition, the spin multiplicities of ground states are mostly 4, 5 and 6 (6 for the CrN_n clusters (CrN_3, CrN_5 and CrN_{11}) possessing N_3 ligand) for neutral CrN_n clusters, and the symmetries of ground states in the large-sized CrN_n clusters decreases to C_1 symmetry, except for CrN_{10} cluster. However, unlike the neutral clusters, the geometries of ground state cationic isomers exhibit relatively high symmetries with spin multiplicities of 3 or 6, which suggest that the loss of one electron in large-sized chromium–nitrogen clusters can result in enhanced symmetry.

To estimate the strengths of the interactions between Cr atom and N ligands as well as the relative stabilities among the $CrN_n^{0/+}$ clusters, we have calculated the average binding energy and the second-order difference. The average binding energy E_b serves as an effective criterion for assessing the thermodynamic stability of cluster, while the second-order difference $\Delta^2 E$ is a crucial parameter reflecting the relative stability between adjacent clusters. The average binding energy and second-order difference values are calculated as below:

$$E_b(CrN_n^{0/+}) = 2[E(Cr^{0/+}) + n/2E(N_2) - E(CrN_n^{0/+})]/n \quad (1)$$

$$\Delta^2 E(CrN_n^{0/+}) = E(CrN_{n+1}^{0/+}) + E(CrN_{n-1}^{0/+}) - 2E(CrN_n^{0/+}) \quad (2)$$

where $E(Cr^{0/+})$ and $E(N_2)$ denote the energies of Cr atom (or Cr^+ cation) and N_2 ligands, respectively, and $E(CrN_n^{0/+})$ represents the total energy of $CrN_n^{0/+}$ clusters. According to eqn (1), the calculated E_b values are presented in Table 1 and Fig. 4(a). The binding energy of the ground state of CrN_8^+ cluster is 0.70 eV. It is noteworthy that the energy of photon in 266 nm laser is about 4.67 eV, which exceeds the energy required for the dissociation of CrN_8^+ cluster into Cr^+ cation and four N_2 molecules (2.79 eV). It is in good agreement with the observation of Cr^+ cation mass spectra peaks in the photolysis experiments. However, a small amount of CrN_2^+ is still present in the photolysis products, which suggests potential factors influencing the experiments, such as the photon absorption cross section of the clusters. The calculated average binding energies are consistent with the photolytic experiments, thereby confirming that the current cluster structure searches of chromium–nitrogen clusters are reliable and the ground state structures are indeed the true local minima for respective cluster sizes.

The E_b curves show odd–even oscillations for both neutral and cationic chromium–nitrogen clusters with the increase of cluster sizes. E_b is positive when n is even, otherwise it is
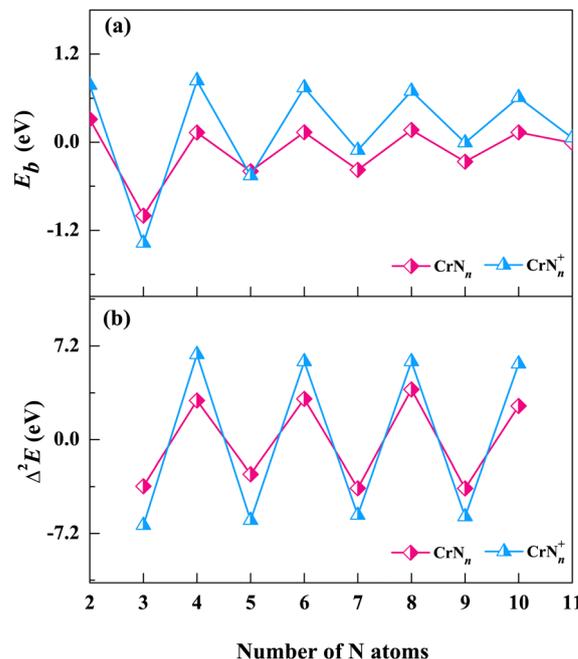

Fig. 4 The average binding energy E_b and the second order difference $\Delta^2 E$ of the low-lying isomers of $CrN_n^{0/+}$ clusters. (a) average binding energy and (b) second order difference.

negative. The negative values indicate the absorption of the energies. Notably, the prominent peaks appear at n = even, and the peaks for cationic clusters are higher than those of neutral clusters. The odd–even oscillations observed in the E_b curves of $CrN_n^{0/+}$ clusters are attributed to the interplay of quantum mechanical effects, particularly the shell structures of clusters. This phenomenon arises due to the quantization of energy levels associated with the discrete arrangement of Cr atom/cation within the $CrN_n^{0/+}$ clusters. In $CrN_n^{0/+}$ clusters with an even number of N atoms, such as n = 4, 6, 8, 10, the presence of the unpaired Cr atom/cation leads to enhanced stability, as the unpaired Cr atom/cation occupies a lower energy level, resulting in a higher average binding energy. Meanwhile, geometric analyses reveal that the low-lying isomers of $CrN_n^{0/+}$ clusters predominantly adopt conformations of $Cr(N_2)_{n/2}$ (or $Cr^+(N_2)_{n/2}$) when n is even, which suggests the propensities of Cr atom/cation in both neutral and cationic chromium–nitrogen clusters readily interact with N_2 ligands, resulting in the formation of stable structures. It is worth noting that, except for n = 3 and 5, the E_b of cationic clusters are higher than those of the corresponding neutral clusters, especially pronounced when n = even. This observation implies that the removal of one electron enhances the stability of the most chromium nitrogen clusters.

The second-order difference values, calculated according to eqn (2), are presented in Table 1 and Fig. 4(b). The second-order difference curve also exhibits the obvious trend of odd–even oscillations, which is consistent with the average binding energy curves. Similarly, the significant peaks on the second-order difference curves are located at the points where n is even, with cationic clusters displaying greater amplitude of

14542 | *Phys. Chem. Chem. Phys.*, 2024, **26**, 14538–14546

This journal is © the Owner Societies 2024

oscillations. In cationic chromium–nitrogen clusters, the maximum value of $\Delta^2 E$ is 6.55 eV (CrN_4^+), followed by 6.00 eV (CrN_8^+). In neutral clusters, the maximum value is 3.87 eV (CrN_8). The calculated results of both cationic and neutral clusters show that the chromium–nitrogen clusters with even number of N atoms are more stable in comparison to their adjacent clusters, reconfirming the stabilities of clusters containing the N_2 units are more stable than those containing the single N atom. However, mass spectral results reveal that CrN_9^+ and CrN_{11}^+ with an odd number of N atoms also exhibit relatively high intensities in their mass spectral peaks, which is possibly attributed to their "kinetically easier formation" under the present reaction conditions. In addition, the HOMO–LUMO gap (HLG) is another important parameter to describe the thermodynamic stability of cluster, which reflects the energy required for the electron to transition from the HOMO to the LUMO, $i.e.$, the energy needed for an excited state transition. The HLGs of $CrN_n^{0/+}$ clusters are listed in Table S3 of the ESI.† It can be seen that the HLGs of CrN_8^+ clusters are 8.23 eV and 13.33 eV for α and β orbitals, respectively, indicating their remarkable stabilities.

We next explore the electronic structures of $CrN_n^{0/+}$ (n = 2–11) clusters by assessing the charge transfer of Cr atoms (or Cr^+ cations) using natural population analysis (NPA). The natural charges on Cr atoms (or Cr^+ cations) are determined for structures corresponding to the lowest energy isomers. As shown in Fig. 5, the charge curve of Cr atom is positive (between 0 and 1) for neutral CrN_n clusters, except for CrN_4. The most notable peaks occur at n = 3, 5 and 11, and the Cr atoms in these clusters are observed to interact with the N_3 ligand. The Cr^+ cation charge distributions of cationic CrN_n^+ clusters are also positive in the range of 0 to 1, except for n = 3, which show gradual decrease with n increasing. These results indicate that Cr atoms easily lose electrons in neutral CrN_n clusters, on the contrary, the Cr^+ cations in CrN_n^+ clusters are more likely to gain electrons. Notably, for n = 2, CrN_2 and CrN_2^+ clusters share the same geometrical configuration of linear Cr–N–N. However, the charge of Cr atom in CrN_2 cluster is 0, while the charge of Cr^+ cation in CrN_2^+ cluster is approximately 1, which suggests the more charge exchanges between the N_3 ligand and the Cr atom compared to
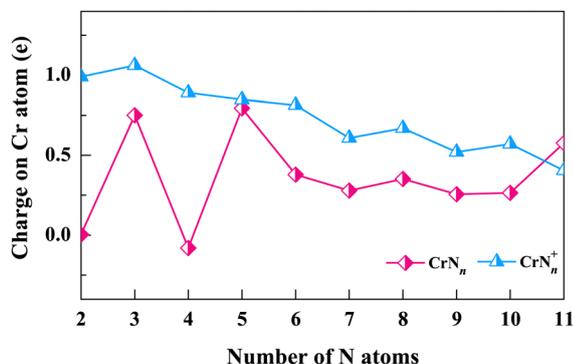
the N_2 ligand. The NPA results suggest that the factors such as the cluster size, the N ligand configurations, and the oxidation states of Cr (neutral or cationic) in $CrN_n^{0/+}$ (n = 2–11) clusters are likely to influence the interactions and charge transfers between Cr atoms (or Cr^+ cations) and N ligands.

Our experimental mass spectra of CrN_n^+ (n = 2–11) clusters reveal the predominant presence of the CrN_8^+ cluster. Additionally, the comprehensive theoretical analyses of the relative stabilities of $CrN_n^{0/+}$ (n = 2–11) clusters demonstrate that the CrN_8^+ cluster exhibits high D_2 symmetry and excellent stability. Thus, we selected CrN_8^+ cluster as an example to explore the molecular orbitals and the chemical bonding patterns of chromium doped nitrogen clusters. Clearly, the CrN_8^+ cluster is open-shell structure. The diagrams of the highest occupied molecular orbital (HOMO) and the lowest unoccupied molecular orbital (LUMO) as well as their eigenvalues with nearest-neighbor molecular orbitals (MOs) of CrN_8^+ cluster are displayed in Fig. 6. The representations are segregated into α- (spin-up) and β-orbitals (spin-down). The HOMO–LUMO gap for CrN_8^+ cluster is 8.23 and 13.33 eV for α- and β-orbitals, respectively. In α-MOs, both LUMOs and HOMOs of CrN_8^+ cluster are triple degeneration. The LUMOs are mainly contributed by N-2p atomic orbitals (AOs), especially $2p_x$, while Cr AOs contribute only 19.07–19.25%. The HOMOs are contributed by Cr-3d orbitals (88.93–88.98%), particularly $3d_{xy}$. Similarly, in β-MOs, triple degenerate LUMOs and HOMOs are also observed. The β-LUMOs are mainly contributed by Cr-AOs with 4p orbitals accounting for 35.71–36.06% and 3d orbitals for 14.59–14.75%. The largest contribution to β-HOMOs is the N-2p orbitals, with Cr-AOs accounting for only 2.67–2.68%. As mentioned above, the triple degeneracy of LUMOs and HOMOs at the α and β orbitals of cationic CrN_8^+ cluster is attributed to the fourfold collocation of Cr^+ ion with the D_2 symmetry, which leads to the splitting of the Cr^+-4p orbitals into the triple degenerate p_x, p_y, and p_z orbitals and the Cr^+-3d orbitals into

Fig. 5 Charges on the Cr atoms (or Cr^+ cations) in the ground state structures of $CrN_n^{0/+}$ clusters.
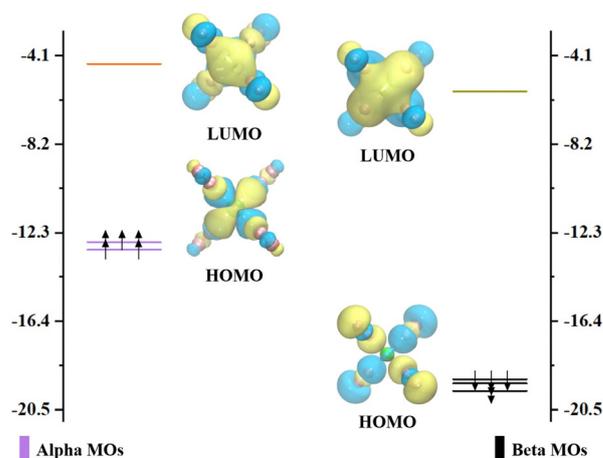

Fig. 6 The molecular orbitals of the ground state structure of CrN_8^+ cluster. The purple and black lines indicate positions of the occupied α and β orbitals, while the orange and green lines indicate the unoccupied α and β orbitals, respectively.

This journal is © the Owner Societies 2024

Phys. Chem. Chem. Phys., 2024, **26**, 14538–14546 | **14543**
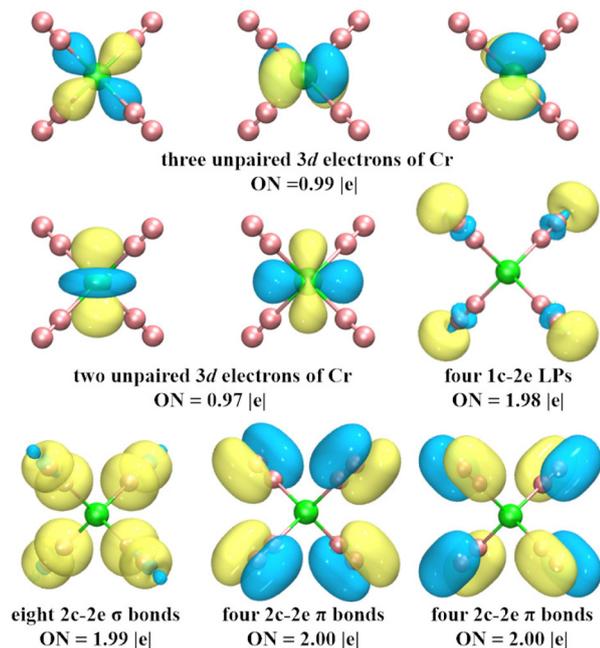
Fig. 7 AdNDP analysis of the ground state structure of CrN_8^+ cluster. ON indicates the number of occupied electrons.

the triple degenerate d_{xy}, d_{xz}, and d_{yz} orbitals, as well as the double degenerate $d_{x^2-y^2}$ and d_{z^2} orbitals. However, as shown in Fig. S4 (ESI†), no degeneracy orbitals appear in the MOs of neutral CrN_8 cluster. It is found that the neutral CrN_8 cluster possesses an additional electron in comparison to CrN_8^+ cluster, which induces the Jahn–Teller effect. The loss of an electron from the neutral CrN_8 cluster leads to the degeneracy of AOs and the increase of the HLG values in CrN_8^+ cluster. Meanwhile, the symmetry changes from D_2 to C_S. The stability of CrN_8^+ cluster is attributed to the strong interactions between the Cr-3d AOs and the N-2p AOs.

To explore the chemical bonding of CrN_8^+ cluster, the multicenter chemical bonds between Cr^+ cation and N atoms are analyzed by AdNDP method. The multicenter bonding is denoted as the xc–2e, where x denotes the number of centers involved (x can range from one center (*i.e.*, alone electrons on single atom) to the maximum number of atoms in the cluster (*i.e.*, fully delocalization bonding)), and ON denotes the number of electrons occupying the cluster, with an ideal value of 2.00 |e|. The AdNDP results (Fig. 7) show that the chemical bonding patterns of CrN_8^+ clusters can be categorized into: five localized spin orbitals (LSOs) occupied by a single electron, four lone pairs (LPs), and 16 two center–two electron bonds (2c–2e). The five 3d subshell layers are occupied by Cr-3d electrons. These LSOs exhibit inert characteristics, devoid of participating in the chemical bonding. The four LPs with ON = 1.98 |e| mainly comprise 2s electrons of N atoms. The sixteen 2c–2e bonds, with ON values approximating the ideal value of 2.00 |e|, contain three types of bonds: the N–N σ bond, the N–N π bond, and the Cr–N σ bond. Among them, eight N–N π-bonds and four N–N σ-bonds contribute to the chemical bonding between the N_2 units, while the remaining four σ-bonds

between Cr and N describe the strong chemical bonds between the central Cr cation and the N_2 units. These bonds are collectively responsible for the stability of cationic CrN_8^+ cluster. In addition, the chemical bonding patterns of neutral CrN_8 cluster are shown in Fig. S5 (ESI†). Similarly, the fifteen 2c–2e bonds of CrN_8 cluster are divided into three bonding modes, *i.e.* N–N σ bonds, N–N π bonds, and Cr–N σ bonds. Thus, it can be inferred that the presence of strong chemical bonds between Cr cation and N_2 ligands enhances the stability of cationic CrN_8^+ cluster.

4 Conclusions

In summary, we have produced chromium heteroazide clusters, namely CrN_6^+, CrN_8^+, CrN_9^+, and CrN_{11}^+, using laser sputtering techniques. The photodissociation results indicate the remarkable abundance of CrN_8^+ cluster compared to other chromium–nitrogen clusters. Subsequently, we have systematically studied the geometrics, stabilities and electronic properties of $CrN_n^{0/+}$ clusters (n = 2–11) by CALYPSO cluster structural search method and DFT calculations at the M06-2X/6-311+G(d,p) level. The obtained ground state structures of cationic chromium–nitrogen clusters are in good agreement with the mass spectra experiments. The calculated results reveal that the isomer with multiple N_2 units tend to possess relatively lower energy than those with all-nitrogen units in chromium–nitrogen clusters. Cationic CrN_n^+ (n = 2–11) clusters, upon electron loss, exhibit enhanced symmetry and stability, especially for CrN_8^+ (^{6}A, D_2) cluster. Most ground state structures conform to configurations of $Cr^{0/+}$ $(N_2)_{n/2}$ and $Cr^{0/+}$ $N(N_2)_{(n-1)/2}$. Molecular orbital analyses of $CrN_8^{0/+}$ clusters elucidate the emergence of the Jahn–Teller effect, primarily influenced by the interactions of the Cr-3d and N-2p orbitals. This effect is accompanied by a notable elevation in the HOMO–LUMO gap of cationic CrN_8^+ cluster. These results provide valuable insights for understanding the structural evolutions, chemical bonding and growth mechanisms of Cr doped nitrogen clusters, which provide an important avenue for the design and synthesis of novel transition metal nitrides.

Conflicts of interest

There are no conflicts to declare.

Acknowledgements

References

1 H. Hu, X. Wang, J. P. Attfield and M. Yang, Metal nitrides for seawater electrolysis, *Chem. Soc. Rev.*, 2024, **53**, 163–203.

2 Y. Y. Wang, S. Liu, S. C. Lu, Y. Li and Z. Yao, Nitrogen-rich Ce-N compounds under high pressure, *Phys. Chem. Chem. Phys.*, 2024, **26**, 9601–9607.

3 C. Zhang, C. Sun, B. Hu, C. Yu and M. Lu, Synthesis and characterization of the pentazolate anion cyclo-N_5^- in $(N_5)_6(H_3O)_3(NH_4)_4Cl$, *Science*, 2017, **355**, 374–376.

4 S. Chu and A. Majumdar, Opportunities and challenges for a sustainable energy future, *Nature*, 2012, **488**, 294–303.

5 M. Bykov, S. Chariton, E. Bykova, S. Khandarkhaeva and T. Fedotenko, *et al.*, High-pressure synthesis of metal-inorganic frameworks Hf_4N_{20} center dot N_2, WN_8 center dot N_2, and Os_5N_{28} center dot $3N_2$ with polymeric nitrogen linkers, *Angew. Chem., Int. Ed.*, 2020, **59**(26), 10321–10326.

6 D. Laniel, B. Winkler, E. Koemets, T. Fedotenko, M. Bykov, E. Bykova, L. Dubrovinsky and N. Dubrovinskaia, Synthesis of magnesium-nitrogen salts of polynitrogen anions, *Nat. Commun.*, 2019, **10**, 4515.

7 S. Lin, J. Chen, B. Zhang, J. Hao, M. Xu and Y. Li, Lanthanium nitride LaN_9 featuring azide units: the first metal nine-nitride as a high-energy-density material, *Phys. Chem. Chem. Phys.*, 2024, **26**, 3605–3613.

8 S. Niu, Y. Liu, Z. Yang, S. Liu and Z. Yao, Prediction of metastable phase of the Sc-N system in the N-rich region under high pressure, *Phys. Chem. Chem. Phys.*, 2023, **25**, 20009–20014.

9 X. Xin, I. Douair, T. Rajeshkumar, Y. Zhao, S. Wang, L. Maron and C. Zhu, Photochemical synthesis of transition metal-stabilized uranium (VI) nitride complexes, *Nat. Commun.*, 2022, **13**, 3809.

10 T. Ye, S. Park, Y. Lu, J. Li, M. Sasase, M. Kitano and H. Hosono, Contribution of nitrogen vacancies to ammonia synthesis over metal nitride catalysts, *J. Am. Chem. Soc.*, 2020, **142**(33), 14374–14383.

11 L. P. Cheng and Q. S. Li, N_4 ring as a square planar ligand in novel MN_4 species, *J. Phys. Chem. A*, 2005, **109**, 3182–3186.

12 R. Haiges, J. A. Boatz, T. Schroer, M. Yousufuddin and K. O. Christe, Experimental evidence for linear metal-azido coordination: the binary group 5 azides $[Nb(N_3)_5]$, $[Ta(N_3)_5]$, $[Nb(N_3)_6]^-$, and $[Ta(N_3)_6]^-$, and 1:1 acetonitrile adducts $[Nb(N_3)_5(CH_3CN)]$ and $[Ta(N_3)_5(CH_3CN)]$, *Angew. Chem., Int. Ed.*, 2006, **45**, 4830–4835.

13 R. Haiges, J. A. Boatz, M. Yousufuddin and K. O. Christe, Monocapped trigonal-prismatic transition-metal heptaazides: syntheses, properties, and structures of $[Nb(N_3)_7]^{2-}$ and $[Ta(N_3)_7]^{2-}$, *Angew. Chem., Int. Ed.*, 2007, **46**, 2869–2874.

14 R. Haiges, J. A. Boatz and K. O. Christe, The syntheses and structure of the vanadium(IV) and vanadium(V) binary azides $V(N_3)_4$, $[V(N_3)_6]^{2-}$, and $[V(N_3)_6]^-$, *Angew. Chem., Int. Ed.*, 2010, **49**, 8008–8012.

15 R. Haiges, J. A. Boatz, R. Bau, S. Schneider, T. Schroer, M. Yousufuddin and K. O. Christe, Polyazide chemistry: the first binary group 6 azides, $Mo(N3)6$, $W(N3)6$, $[Mo(N3)7]-$, and $[W(N3)7]-$, and the $[NW(N3)4]-$ and $[NMo(N3)4]-$ ions, *Angew. Chem., Int. Ed.*, 2005, **117**(12), 1894–1899.

16 C. Knapp and J. Passmore, On the way to "solid nitrogen" at normal temperature and pressure? binary azides of heavier group 15 and 16 elements, *Angew. Chem., Int. Ed.*, 2004, **43**, 4834–4836.

17 L. Gagliardi and P. Pyykkö, Scandium cycloheptanitride, ScN_7: a predicted high-energy molecule containing an $[\eta^7-N_7]^{3-}$ ligand, *J. Am. Chem. Soc.*, 2001, **123**, 9700–9701.

18 Q. S. Li and H. X. Duan, Density functional theoretical study of a series of binary azides $M(N_3)_n$ ($n = 3, 4$), *J. Phys. Chem. A*, 2005, **109**, 9089–9094.

19 J. Müller, Azides of the heavier Group 13 elements, *Coord. Chem. Rev.*, 2002, **235**, 105–119.

20 R. Haiges, J. A. Boatz, J. M. Williams and K. O. Christe, Preparation and characterization of the binary group 13 azides $M(N3)3$ and $M(N3)3CH3$ CN (M = Ga, In, Tl), $[Ga(N3)5]2-$, and $[M(N3)6]3-$ (M = In, Tl), *Angew. Chem., Int. Ed.*, 2011, **123**, 8990–8995.

21 L. Gagliardi and P. Pyykkö, Predicted group 4 tetra-azides $M(N_3)_4$ (M = Ti-Hf, Th): the first examples of linear M-NNN coordination, *Inorg. Chem.*, 2003, **42**, 3074–3078.

22 M. Straka, N_6 ring as a planar hexagonal ligand in novel $M(\eta^6-N_6)$ species, *Chem. Phys. Lett.*, 2002, **358**, 531–536.

23 H. X. Duan and Q. S. Li, A series of novel aromatic compounds with a planar N_6 ring, *Chem. Phys. Lett.*, 2006, **432**, 331–335.

24 C. Sun, C. Zhang, C. Jiang, C. Yang, Y. Du, Y. Zhao, B. Hu, Z. Zheng and K. O. Christe, Synthesis of AgN_5 and its extended 3D energetic framework, *Nat. Commun.*, 2018, **9**, 1269.

25 Y. Wang, M. Bykov, I. Chepkasov, A. Samtsevich, E. Bykova, X. Zhang, S. Q. Jiang, E. Greenberg, S. Chariton and V. B. Prakapenka, Stabilization of hexazine rings in potassium polynitride at high pressure, *Nat. Chem.*, 2022, **14**, 794–800.

26 D. Laniel, F. Trybel, Y. Yin, T. Fedotenko, S. Khandarkhaeva, A. Aslandukov, G. Aprilis, A. I. Abrikosov, T. Bin Masood and C. Giacobbe, Aromatic hexazine $[N_6]^{4-}$ anion featured in the complex structure of the high-pressure potassium nitrogen compound K_9N_{56}, *Nat. Chem.*, 2023, **15**, 641–646.

27 K. Ding, T. Li, H. Xu, Y. Li, Z. Ge, W. Zhu and W. Zheng, Mass spectrometry detection of LiN_{12}^+ cluster and theoretical investigation of its structures and stability, *Chem. Phys. Lett.*, 2020, **747**, 137310.

28 Z. Ge, K. Ding, Y. Li, H. Xu, Z. Chen, Y. Ma, T. Li, W. Zhu and W. Zheng, Structural evolution of LiN_n^+ ($n = 2, 4, 6, 8,$ and 10) clusters: mass spectrometry and theoretical calculations, *RSC Adv.*, 2019, **9**(12), 6762–6769.

29 K. Ding, T. Li, X. Hongguang, P. Jian, Y. Bin, W. Zheng and Z. Ge, Generation and detection of sodium heteronitrogen clusters with high nitrogen content, *Chin. J. Explos. Propellants*, 2020, **28**, 597–602.

30 T. Li, K. Ding, H. Xu, L. Qin, Q. Chen, W. Zheng and Z. Ge, Laser sputtering method for generating alkali metal heteronitrogen clusters NaN_n^+ and KN_n^+, *Chem. Wld.*, 2021, **60**(1), 28–32.

This journal is © the Owner Societies 2024

Phys. Chem. Chem. Phys., 2024, **26**, 14538–14546 | **14545**

31 T. Li, K. Ding, H. Xu, L. Qian, J. Xiao, W. Zhu and Z. Ge, Formation and photodissociation of Cr doped nitrogen clusters CrN_n^+, *Chin. J. Explos. Propellants*, 2017, **40**(06), 55–58.

32 K. Ding, H. Xu, Y. Yang, T. Li, C. Zhao, Z. Ge, W. Zheng and W. Zhu, Mass spectrometry and theoretical investigation of VN_n^+ ($n = 8$, 9, and 10) clusters, *J. Phys. Chem. A*, 2018, **122**, 4687–4695.

33 K. Ding, L. Xiao, H. Xu, T. Li, Z. Ge, W. Qian and W. Zhu, Experimental observation of TiN_{12}^+ cluster and theoretical investigation of its stable and metastable isomers, *Chem. Sci.*, 2015, **6**, 4723–4729.

34 K. Ding, H. Chen, H. Xu, B. Yang, Z. Ge, C. Lu and W. Zheng, Identification of octahedral coordinated ZrN_{12}^+ cationic clusters by mass spectrometry and structure searches, *Dalton Trans.*, 2021, **50**, 10187–10192.

35 T. Li, K. Ding, L. Hong, P. Jian, Y. Bin, L. Wei and Z. Ge, Formation and laser photolysis of metal-doped nitrogen clusters FeNn+, CoNn+ and NiNn+, *Chin. J. Explos. Propellants*, 2022, **40**, 200–204.

36 S. M. Casey and D. G. Leopold, Negative ion photoelectron spectroscopy of chromium dimer, *J. Phys. Chem.*, 1993, **97**, 816–830.

37 K. Andersson, The electronic spectrum of Cr_2, *Chem. Phys. Lett.*, 1995, **237**, 212–221.

38 G. Gewinner, J. C. Peruchetti, A. Jaegle and A. Kalt, Photoemission study of the chromium (111) surface interacting with oxygen, *Surf. Sci.*, 1978, **78**, 439–458.

39 T. Jiang, I. Odnevall Wallinder and G. Herting, Chemical stability of chromium carbide and chromium nitride powders compared with chromium metal in synthetic biological solutions, *Int. Scholarly Res. Not.*, 2012, **2012**, 379697.

40 Z. Schauperl, V. Ivušić and B. Runje, Wear resistance of chromium-nitride and diamond-like carbon thin hard coatings, *Mater. Test.*, 2008, **50**, 326–331.

41 M. Khan, W. Cao, N. Chen, U. Asad and M. Z. Iqbal, *Ab initio* calculations of synergistic chromium-nitrogen codoping effects on the electronic and optical properties of anatase TiO_2, *Vacuum*, 2013, **92**, 32–38.

42 Q. Wang, Q. Sun, B. K. Rao, P. Jena and Y. Kawazoe, Nitrogen-induced magnetic transition in small chromium clusters, *J. Chem. Phys.*, 2003, **119**, 7124–7130.

43 Y. C. Zhao, Z. G. Zhang, J. Y. Yuan, H. G. Xu and W. J. Zheng, Modification of reflectron time-of-flight mass spectrometer for photodissociation of mass-selected cluster ions, *Chin. J. Chem. Phys.*, 2009, **22**, 655–662.

44 J. Lv, Y. Wang, L. Zhu and Y. Ma, Particle-swarm structure prediction on clusters, *J. Chem. Phys.*, 2012, **137**, 084104.

45 Y. Wang, J. Lv, L. Zhu and Y. Ma, CALYPSO: A method for crystal structure prediction, *Comput. Phys. Commun.*, 2012, **183**, 2063–2070.

46 Y. Wang, J. Lv, L. Zhu and Y. Ma, Crystal structure prediction *via* particle swarm optimization, *Phys. Rev. B: Condens. Matter Mater. Phys.*, 2010, **82**, 7174–7182.

47 B. L. Chen, K. H. He, W. Dai, G. L. Gutsev and C. Lu, Geometric and electronic diversity of metal doped boron clusters, *J. Phys.: Condens. Matter*, 2023, **35**, 183002.

48 J. N. Zuo, L. L. Zhang, B. L. Chen, K. H. He, W. Dai, K. W. Ding and C. Lu, Geometric and electronic structures of medium-sized boron clusters doped with plutonium, *J. Phys.: Condens. Matter*, 2023, **36**, 015302.

49 B. L. Chen, L. J. Conway, W. Sun, X. Kuang, C. Lu and A. Hermann, Phase stability and superconductivity of lead hydrides at high pressure, *Phys. Rev. B*, 2021, **103**, 035131.

50 C. Lu, C. Cui, J. Zuo, H. Zhong, S. He, W. Dai and X. Zhong, Monolayer $ThSi_2N_4$: an indirect-gap semiconductor with ultra-high carrier mobility, *Phys. Rev. B*, 2023, **108**, 205427.

51 Q. Duan, L. Zhan, J. Shen, X. Zhong and C. Lu, Predicting superconductivity near 70 K in 1166-type boron-carbon clathrates at ambient pressure, *Phys. Rev. B*, 2024, **109**, 054505.

52 B. L. Chen, K. H. He, W. Dai, G. L. Gutsev and C. Lu, Geometric and electronic diversity of metal doped boron clusters, *J. Phys.: Condens. Matter*, 2023, **35**, 183002.

53 W. M. Haynes, *CRC handbook of chemistry and physics*, CRC press, 2014.

54 D. Y. Zubarev and A. I. Boldyrev, Developing paradigms of chemical bonding: adaptive natural density partitioning, *Phys. Chem. Chem. Phys.*, 2008, **10**, 5207–5217.

55 M. J. Frisch, G. W. Trucks, H. B. Schlegel, G. E. Scuseria, M. A. Robb, J. R. Cheeseman, J. A. Montgomery Jr, T. Vreven, K. Kudin, J. Burant, J. M. Millam, S. S. Iyengar, J. Tomasi, V. Barone, B. Mennucci, M. Cossi, G. Scalmani, N. Rega, G. A. Petersson, H. Nakatsuji, M. Hada, M. Ehara, K. Toyota, R. Fukuda, J. Hasegawa, M. Ishida, T. Nakajima, Y. Honda, O. Kitao, H. Nakai, M. Klene, X. Li, J. E. Knox, H. P. Hratchian, J. B. Cross, V. Bakken, C. Adamo, J. Jaramillo, R. Gomperts, R. E. Stratmann, O. Yazyev, A. J. Austin, R. Cammi, C. Pomelli, J. Ochterski, P. Y. Ayala, K. Morokuma, G. A. Voth, P. Salvador, J. J. Dannenberg, V. G. Zakrzewski, S. Dapprich, A. D. Daniels, M. C. Strain, O. Farkas, D. K. Malick, A. D. Rabuck, K. Raghavachari, J. B. Foresman, J. V. Ortiz, Q. Cui, A. G. Baboul, S. Clifford, J. Cioslowski, B. B. Stefanov, G. Liu, A. Liashenko, P. Piskorz, I. Komaromi, R. L. Martin, D. J. Fox, T. Keith, M. A. Al-Laham, C. Y. Peng, A. Nanayakkara, M. Challacombe, P. M. W. Gill, B. G. Johnson, W. Chen, M. W. Wong, C. Gonzalez and J. A. Pople, *Gaussian 09, A.02*, Gaussian, Inc., Wallingford CT, 2009.

14546 | *Phys. Chem. Chem. Phys.*, 2024, **26**, 14538–14546

This journal is © the Owner Societies 2024